https://doi.org/10.1016/j.nanoen.2022.107398

Neighboring effects of active sites for CO_2 transition to C_1 products on atomic catalysts

Mingzi Sun[1], Bolong Huang[1,2,3,4,*]

[1]Department of Applied Biology and Chemical Technology, The Hong Kong Polytechnic University, Hung Hom, Kowloon, Hong Kong SAR, China
[2]Beijing Institute of Nanoenergy and Nanosystems, Chinese Academy of Sciences, Beijing 100083, China
[3]Research Institute for Smart Energy (RISE), The Hong Kong Polytechnic University, Hung Hom, Kowloon, Hong Kong SAR, China
[4]Research Institute for Intelligent Wearable Systems (RI-IWEAR), The Hong Kong Polytechnic University, Hung Hom, Kowloon, Hong Kong SAR, China

*Corresponding author. Email: bhuang@polyu.edu.hk

Abstract

The metal sites of single atomic catalysts (SAC) have usually been considered as the only active sites while the neighboring effects are rarely discussed. To enhance our understanding of the reaction mechanisms and the contributions of active sites, we have carried out a detailed investigation to reveal the correlations between the neighboring effects and the thermodynamic reaction trend of CO_2 reduction reactions (CO_2RR). In particular, the CO_2 adsorptions on graphdiyne (GDY) are strongly correlated with the electronic configurations of the anchoring metals, especially for 3d transition metals. Owing to the neighboring effect, the initial adsorption of CO_2 and further reduction process show different preferred active sites, supporting the migration of intermediates during CO_2RR. More importantly, it is found that GDY-lanthanide SACs are able to effectively suppress the neighboring effects to promote the formation of the CH_3OH and CH_4 *via* the metal sites. This work has supplied in-depth insights into the neighboring effects to facilitate the design of efficient atomic catalysts in future works.

Introduction

To address the challenges of the greenhouse effect, converting CO_2 into high value-added chemicals or carbon-based liquid fuels through CO_2 reduction reactions (CO_2RR) has become one of the most promising technology for carbon neutrality [1-2]. This technology still strongly depends on high-efficiency and stable electrocatalyst materials to accomplish different pathways of multi-carbon products[3]. Therefore, designing and fabricating the highly efficient electrocatalysts for CO_2RR is the most critical research task for current research [4-5][10.1007/s12598-021-01728-x]. Many different types of electrocatalysts have been designed and synthesized including metals[6], alloys[7-9], and metal oxides[10-11][10.1007/s12598-021-01774-5], etc., where the noble metal-based electrocatalysts have attracted intensive interest due to remarkable performances[12-13], especially for the Cu-based electrocatalysts[14-18]. As emerging electrocatalysts, single atomic catalysts (SAC) on different supports have possessed great potential for the CO_2RR. In particular, graphdiyne (GDY) based SACs have attracted intensive research interest due to their unique lattice and electronic structures[19-21][10.1093/nsr/nwaa213][10.1002/cphc.202000579]. Although GDY has shown excellent performances in electrocatalysis and photocatalysis [22-24][10.1016/j.nanoen.2020.104667; 10.1016/j.isci.2018.12.006], the application in CO_2RR is still limited[25-26].

To understand the origins of high electroactivity, the regulations and characterizations of active sites in SACs are also significant, which is only limited to the atomically dispersed metal sites. In our previous work, we have successfully proved the charge compensation induced by the strong interactions between GDY and anchoring metals, which further leads to the zero valences of transition atoms for efficient electrocatalysts [20][10.1002/cphc.202000579]. The neighboring sites not only modulate the electronic structures of the anchoring metal sites but also participate in the electrocatalytic process to facilitate the electron transfer, especially for those carbon-supported SACs [10.1038/s41929-018-0203-5; 10.1021/jacs.0c02229; 10.1002/anie.201804817]. However, so far, most of the work still focuses on regulations of metal active sites while the understanding of neighboring non-metal sites is not sufficient. Our previous work has confirmed that the framework of GDY shows the high electroactivity towards the HER, which further revealed that the involvement of carbon sites should be included for GDY-SACs [Accelerating].

Currently, the comprehensive understanding of the reaction mechanism for CO_2RR is still limited since even similar SACs have shown varied electrochemical performances of CO_2RR. Meanwhile, the research of ACs has only been focused on the metal sites while the neighboring effects and electroactivity of support are usually not discussed, leading to the challenges of effective modulations and rational design. To address this challenge, we have carried out systematic explorations on transitions from CO_2 towards different products of C_1 pathways to understand the effect of neighboring on the electroactivity of GDY-SACs covering transition metals (TMs) and lanthanide (Ln) metals. This work has provided an in-depth understanding of the C_1 pathways, which will benefit future explorations to achieve C_{2+} products.

Results and Discussions

CO_2 adsorption on GDY-SACs.

The focus of the active sites is usually only considered in the atomically dispersed metal sites while the neighboring effect is rarely discussed. First, we demonstrate the unique correlation between the formation energy of SAC and CO_2 adsorption on metal sites (**Figure 1a-b**). For the formation energies, GDY-TMs SACs show a similar trend with a volcano pattern of change, which is similar to the CO_2 adsorption in GDY-3d,4d TMs SACs. It is noted that for late-3d

TMs based GDY-SACs (after d^6 electronic configurations), the formation energy of SAC and CO_2 adsorption shows an opposite trend, which is attributed to the electron transfer from metal towards CO_2. Interestingly, for the GDY-5d TMs SACs, the CO_2 adsorption energies are directly opposite to the thermodynamic stability of GDY-SACs, supporting the chemisorption of CO_2 due to the much weaker constraint of 5d orbitals. Similar to 5d TMs, GDY-Ln SACs also support the full chemisorption trends to the CO_2, which is induced by the activation of 5d orbitals in Ln *via* f-d orbitals couplings. Notably, the most stable adsorption of CO_2 locates on the carbon sites rather than the metal sites, which indicates that initial active sites for CO_2RR prefer the alkyl chains of GDY, supporting the existence of the neighboring effects. Therefore, we have also demonstrated the correlation between the selectivity of CO_2 adsorption and the formation energies. Interestingly, we have noticed that the formation energies of the GDY-SACs have shown an overall opposite trend to the adsorption of CO_2 of the most stable structural configurations (**Figure S1a-d**). This reveals that the higher stability of the GDY-SACs leads to the lower electroactivity of the GDY structures. The less stable GDY-SACs are induced by the strong interactions between the GDY support and the metal, which activates the electroactivity of the alkyl chains of the GDY, especially the carbon site C1 and C2 sites near the anchoring metals. This is distinct from the trends in **Figure 1**, supporting that neighboring effects play a significant role in CO_2 adsorption.

Then, the neighboring effects have been further investigated by site-independent adsorptions regarding five carbon sites (C1-C5) and the single metal sites (M1) of the GDY (**Figure 1c-1h**). Middle TMs based GDY-SAC show relatively high energy costs of CO_2 adsorption, leading to the HER performance in our previous work [20]. For 3d TMs, the adsorption energies between the metal and neighboring carbon sites are relatively small, which weakens the selectivity toward specific active sites. GDY-Cu SAC displays an optimal CO_2 adsorption strength, which shows nearly zero on all the sites, which is beneficial to realize the C_{2+} pathways of CO_2RR. Evidently, early TMs based GDY-SACs cause the overbinding effect due to the docking of CO_2 orbitals on the empty d orbitals, which shows the absence of electron transfer. For most sites, the adsorption energies of late TMs have been increased due to the chemisorption of CO_2 with efficient electron transfer from GDY-SAC towards CO_2. For 4d,5d TMs, and Ln metals, the preference for CO_2 adsorption become more evident since the C1-C4 sites show the dominant advantages in the energy cost over the metal and C5 sites. In particular, CO_2 shows highly preferred adsorption on the alkyl chains of GDY-Ln ACs without overbinding effect.

To achieve a more explicit demonstration of the adsorption energy evolution, we have arranged the adsorption energies in the volcano plot (**Figure S2**). The adsorption of CO_2 on different active sites exhibits a similar trend. For GDY-3d TMs SACs, the most stable adsorptions are mainly dominated by the early TMs (Sc, Ti, V) (**Figure S2a**). In the meantime, the mid-TMs based GDY-SACs (Fe, Co, Ni) always show the most unstable adsorptions of CO_2. Notably, although different active sites show a similar trend, the most stable adsorption of CO_2 occurs on the carbon sites, supporting the existence of neighboring effects. The volcano plots further show that the energy trend becomes more similar for GDY-4d,5d TMs SACs (**Figure S2b-c**). However, the most preferred TMs show distinct results from the GDY-3d TMs SACs. Moreover, the energy differences between different active sites are alleviated, leading to the suppression of neighboring effects. For GDY-Ln SACs, the adsorption energies intrinsically show the continuous volcano plot, where the mid-Ln based GDY-SACs always show the most stable adsorptions for CO_2 (**Figure S2d**). These results have indicated that the overall adsorption trends are affected by the overall electronic structures, which is attributed to the introduction of anchoring metals. In the meantime, the interactions between the anchoring metals and GDY

lead to the neighboring effect, which results in the difference in adsorption energies among different active sites.

Reaction pathways of CO_2 transition to C_1 products.

Furthermore, the neighboring effect has been systematically studied through the different C_1 reaction pathways. Since both formations of CO and HCOOH both involve two electrons, the preference for the competitive reactions has been demonstrated (**Figure 2** and **Figure S3**). For the competitive formation of HCOOH and CO, we notice the formation of HCOO* shows an overall lower energy cost than that of COOH* on GDY-3d TMs SACs (**Figure 2a-b**). More importantly, the metal sites become the most promising active sites, especially for CO formation. This distinct trend with the CO_2 adsorption indicates the potential migration of CO_2 during the reduction process induced by the neighboring effect. For 4d TMs, although the overall energy costs have increased for both reaction pathways, the metal sites still show a much stronger preference for the HCOOH and CO than other carbon sites. Owing to the lower reaction energy costs of CO, GDY-4d TMs SACs facilitate the formation of CO, especially for Tc to Pd. Similar trends have been noticed for 5d TMs as well, however, only limited GDY-5d TMs are able to realize the HCOOH formation. In contrast, the neighboring effect has been largely suppressed on GDY-Ln SACs (**Figure 2c-2d**). Notably, GDY-Pr and GDY-Pm show distinct reaction energy costs, where the neighboring effect is obvious, resulting in the favored reactions for all active sites. However, the subtle energy cost difference leads to the entangled competition of CO and HCOOH on GDY-Ln SACs. The further hydrogenation of CO leads to the formation of CH_3OH and CH_4, which also deliver the reveals the different levels of neighboring effect. For the formation of CH_3OH supplied in previous work[27], the hydrogenation to form CHO* shows an evident neighboring effect, where the preference between carbon and metals sites is difficult to distinguish (**Figure S3a-c**). However, for the following reaction, we notice that the formation of CH_3OH is strongly hindered due to the high energy costs on both carbon and metals sites. In contrast, metal sites of GDY-Ln SAC are possible candidates to realize the CH_3OH production through the suppression of neighboring effects (**Figure S3d**).

The formation of CH_4 requires the largest electron transfer, which usually leads to strong challenges. The GDY-3d, 5d TMs SACs exhibit the overall lower energy costs (< 1 eV) except for the GDY-Zn (**Figure 3a**). However, the neighboring effect in GDY-3d TMs SACs leads to the limited energy difference between carbon and metal sites. Thus, for GDY-3d TMs, both carbon and metal sites are able to promote the reaction towards CH_4. In particular, GDY-Mn and GDY-Cr SACs are the most promising candidates for CH_4 formation. For GDY-4d TMs SACs, the initial hydrogenation shows much-increased energy barriers (**Figure 3b)**. Distinct from the GDY-3d TMs SACs, metal sites of GDY-4d, 5d TMs SACs become the dominant active sites with downhill reaction trends towards the formation of CH_3*(**Figure 3c)**. Different from the formation of CH_3OH, the challenges appear at the initial hydrogenation to form COH* for nearly all GDY-TMs SACs, where the neighboring effect causes the overall high energy costs on all active sites. From CH_2OH to CH_4, all the hydrogenation steps display continuous uphill energy trends, leading to the decreased conversion efficiency to CH_4. For the formation of CH_4, the formation from CH_3* to CH_4 is the rate-determining step (RDS) with the largest energy barriers, where the GDY-3d,4d TMs SACs show the overall lower barrier of the RDS than GDY-5d TMs SACs (**Figure 3c**). GDY-5d TMs SACs are not promising candidates for the CH_4 formation due to the relatively high energy barriers for nearly all the reaction steps. Compared to TMs, Ln-based GDY-SACs are promising candidates to achieve the formation of CH_3OH (**Figure 3d**). The difficult formation of COH* becomes possible on GDY-Ln SACs, leading to a significantly improved possibility for CH_4 formation. In particular, GDY-Pr, GDY-

Pm, and GDY-Ho SACs show much lower energy costs than other GDY-SACs, supporting the high-performance CO_2RR due to decreased energy barriers for the hydrogenation process even for RDS. Moreover, the much-weakened neighboring effect guarantees the selectivity towards Ln sites during the CO_2RR. These results have unraveled that metal sites are still the dominant active sites to promote the multi-electron reduction of CO_2.

For a long time, the neighboring effect has not been well discussed on SACs. Usually, the thermodynamic results have been used to demonstrate the selectivity of different reactions only on the metal sites as the only active sites. Simply based on the adsorption energies of HCOO* and COOH*, the formation of HCOOH is more preferred than CO, which is different from our previous discussions (**Figure S5a-f**)[27]. The initial hydrogenation is determined by electronic modulation induced by the anchoring metal, where the closer carbon sites exhibit better selectivity after modulations. For the selectivity towards CH_3OH and CH_4, the competitive dehydration and hydrogenation of CHOH* is the key step. Interesting, the dehydrogenation hydration of CHOH* is much more preferred for C1-C4 sites (**Figure S5g-j**). For C5 sites and metal sites, the selectivity did not display strong regulations. This indicates that both neighboring effects and metal selections are critical factors to determine the performance of the CO_2RR (**Figure S5m-n**). Therefore, we have identified that the thermodynamic results cannot comprehensively reveal the active sites and reaction mechanism, where the spatial perturbation induced by the neighboring effect deviates from the reaction process. Although the metal sites are not the most stable adsorption sites for CO_2, they are the dominant active sites to promote the conversion to complicated products, implying the dynamic of CO_2 molecules during the CO_2RR. Therefore, the understanding of the neighboring effect is critical to unraveling the reaction process of CO_2RR, especially the dynamic of CO_2 among different active sites.

Machine learning predictions with neighboring effects.

The advanced machine learning (ML) technique is able to predict the electroactivity of electrocatalysts [28-30] regarding the adsorption energies of different intermediates (**Figure 4a-f**). The neighboring effects have been considered in the ML calculations with fundamental physiochemical properties. Notably, all the predictions and DFT calculations have shown a highly similar trend in the energy change, indicating sufficient accuracy. For the prediction of CO_2, most energies have shown a high prediction accuracy (**Figure 4a**). However, the predictions of CO are relatively dispersive than other intermediates, which is ascribed to the stronger electronic interactions between CO and GDY than inert CO_2 (**Figure 4b**). For both CH_3OH and HCOOH, the results of C2 and C3 sites show the smallest difference between DFT calculations and ML prediction (**Figure 4c-d**). Among different reactants and the products, the predictions of CH_4 show the highest accuracy with the smallest root mean square (RMSE) (**Figure 4e**). In the end, the water adsorption energies are predicted, where the energy change difference is much smaller than other molecules. To highlight the importance of neighboring effects, we have compared the prediction accuracy of machine learning with and without neighboring effects (**Figure S6**). Notably, after the consideration of the neighboring effect, the difference between the machine learning predictions and the DFT calculation data has been significantly reduced, which can be supported by the decreasing RMSE as well. The RMSE of CO_2, CO, HCOOH, CH_3OH, CH_4, and H_2O has been alleviated to 0.0659, 0.10651, 0.04627, 0.05183, 0.02179, and 0.14499, supporting the neighboring effects are important factors for the machine learning predictions. In particular, we notice that the larger molecules (CO_2, HCOOH, CH_3OH, CH_4) show much improved RMSE, where the neighboring effects are relatively weak and several active sites may involve in the adsorption configurations. In comparison, the adsorption of smaller molecules such as CO and H_2O are strongly related to

the active sites, which will be influenced by the neighboring effect evidently. These results have shown that the neighboring effect is a significant factor in understanding electrocatalysis. The deviations of predictions in this work are ascribed to the perturbed electronic structures of GDY and valence states of anchoring metals, especially after the adsorption of different intermediates with strong electron transfer. Therefore, further improvements on the parameterizations and algorithm are still needed in future explorations.

Conclusions

In conclusion, we have clearly unraveled the neighboring effect on GDY-SAC regarding different C_1 pathways of CO_2RR. The electronic configuration of d orbitals determines the adsorption behaviors and electron transfer during the CO_2RR. The distinct thermodynamic trend of CO_2 adsorption and reaction pathways demonstrated the dynamic CO_2 behaviors induced by the neighboring effect. GDY-TMs SACs are promising electrocatalysts for CO and HCOOH while the GDY-Ln SACs show great potential in achieving CH_4 and CH_3OH. Our work indicates that the probing of CO_2RR requires the consideration of both spatial and thermodynamic conditions for a more explicit and comprehensive analysis of the electrocatalysts, which will be highly beneficial in developing efficient SAC to reach multi-carbon products in the future.

Competing interests

The authors declare no competing interests.

Acknowledgments

The authors gratefully acknowledge the support from the National Key R&D Program of China (2021YFA1501101), the NSFC/RGC Joint Research Scheme Project (N_PolyU502/21), and the funding for Projects of Strategic Importance of The Hong Kong Polytechnic University (Project Code: 1-ZE2V).

Reference:

[1] S. Jin; Z. Hao; K. Zhang; Z. Yan; J. Chen, *Angew Chem Int Ed Engl* **2021,** *60* (38), 20627-20648.

[2] A. S. Varela, *Nature Energy* **2021,** *6* (7), 698-699.

[3] D. Gao; R. M. Arán-Ais; H. S. Jeon; B. Roldan Cuenya, *Nature Catalysis* **2019,** *2* (3), 198-210.

[4] S. Nitopi; E. Bertheussen; S. B. Scott; X. Liu; A. K. Engstfeld; S. Horch; B. Seger; I. E. L. Stephens; K. Chan; C. Hahn; J. K. Norskov; T. F. Jaramillo; I. Chorkendorff, *Chem Rev* **2019,** *119* (12), 7610-7672.

[5] A. D. Handoko; F. Wei; Jenndy; B. S. Yeo; Z. W. Seh, *Nature Catalysis* **2018,** *1* (12), 922-934.

[6] H. Xie; T. Wang; J. Liang; Q. Li; S. Sun, *Nano Today* **2018,** *21*, 41-54.

[7] C. Hahn; D. N. Abram; H. A. Hansen; T. Hatsukade; A. Jackson; N. C. Johnson; T. R. Hellstern; K. P. Kuhl; E. R. Cave; J. T. Feaster; T. F. Jaramillo, *Journal of Materials Chemistry A* **2015,** *3* (40), 20185-20194.

[8] L. Jia; M. Sun; J. Xu; X. Zhao; R. Zhou; B. Pan; L. Wang; N. Han; B. Huang; Y. Li, *Angew Chem* **2021,** *133* (40), 21909-21913.

[9] N. Han; M. Sun; Y. Zhou; J. Xu; C. Cheng; R. Zhou; L. Zhang; J. Luo; B. Huang; Y. Li, *Adv Mater* **2021,** *33* (4), e2005821.

[10] S. Liu; J. Xiao; X. F. Lu; J. Wang; X. Wang; X. W. D. Lou, *Angew Chem Int Ed Engl* **2019,** *58* (25), 8499-8503.

[11] S. Liu; X. F. Lu; J. Xiao; X. Wang; X. W. D. Lou, *Angew Chem Int Ed Engl* **2019,** *58* (39), 13828-13833.

[12] A. Klinkova; P. De Luna; C.-T. Dinh; O. Voznyy; E. M. Larin; E. Kumacheva; E. H. Sargent, *ACS Catalysis* **2016,** *6* (12), 8115-8120.

[13] A. Goyal; G. Marcandalli; V. A. Mints; M. T. M. Koper, *J Am Chem Soc* **2020,** *142* (9), 4154-4161.

[14] T. Kim; G. T. R. Palmore, *Nat Commun* **2020,** *11* (1), 3622.

[15] X. Yuan; S. Chen; D. Cheng; L. Li; W. Zhu; D. Zhong; Z. J. Zhao; J. Li; T. Wang; J. Gong, *Angew Chem Int Ed Engl* **2021,** *60* (28), 15344-15347.

[16] M. C. O. Monteiro; F. Dattila; B. Hagedoorn; R. García-Muelas; N. López; M. T. M. Koper, *Nature Catalysis* **2021,** *4* (8), 654-662.

[17] T. Möller; F. Scholten; T. N. Thanh; I. Sinev; J. Timoshenko; X. Wang; Z. Jovanov; M. Gliech; B. Roldan Cuenya; A. S. Varela; P. Strasser, *Angew Chem* **2020,** *132* (41), 18130-18139.

[18] H. Xiao; W. A. Goddard, 3rd; T. Cheng; Y. Liu, *Proc Natl Acad Sci U S A* **2017,** *114* (26), 6685-6688.

[19] Y. Zhao; J. Wan; H. Yao; L. Zhang; K. Lin; L. Wang; N. Yang; D. Liu; L. Song; J. Zhu; L. Gu; L. Liu; H. Zhao; Y. Li; D. Wang, *Nat Chem* **2018,** *10* (9), 924-931.

[20] Y. Xue; B. Huang; Y. Yi; Y. Guo; Z. Zuo; Y. Li; Z. Jia; H. Liu; Y. Li, *Nat Commun* **2018,** *9* (1), 1460.

[21] H. Yu; Y. Xue; B. Huang; L. Hui; C. Zhang; Y. Fang; Y. Liu; Y. Zhao; Y. Li; H. Liu; Y. Li, *iScience* **2019,** *11*, 31-41.

[22] S. Guo; Y. Jiang; F. Wu; P. Yu; H. Liu; Y. Li; L. Mao, *ACS Appl Mater Interfaces* **2019,** *11* (3), 2684-2691.

[23] X. Gao; H. Liu; D. Wang; J. Zhang, *Chem Soc Rev* **2019,** *48* (3), 908-936.

[24] R. Sakamoto; R. Shiotsuki; K. Wada; N. Fukui; H. Maeda; J. Komeda; R. Sekine; K. Harano; H. Nishihara, *Journal of Materials Chemistry A* **2018,** *6* (44), 22189-22194.

[25] C. Zhao; X. Dai; T. Yao; W. Chen; X. Wang; J. Wang; J. Yang; S. Wei; Y. Wu; Y. Li, *J Am Chem Soc* **2017,** *139* (24), 8078-8081.

[26] M. Li; H. Wang; W. Luo; P. C. Sherrell; J. Chen; J. Yang, *Adv Mater* **2020,** *32* (34), e2001848.

[27] M. Sun; H. H. Wong; T. Wu; A. W. Dougherty; B. Huang, *Advanced Energy Materials* **2022,** *12* (14).

[28] M. Sun; A. W. Dougherty; B. Huang; Y. Li; C. H. Yan, *Advanced Energy Materials* **2020**.

[29] M. Sun; T. Wu; A. W. Dougherty; M. Lam; B. Huang; Y. Li; C. H. Yan, *Advanced Energy Materials* **2021,** *11* (13), 2003796.

[30] M. Sun; H. H. Wong; T. Wu; A. W. Dougherty; B. Huang, *Advanced Energy Materials* **2021,** *11* (30), 2101404.

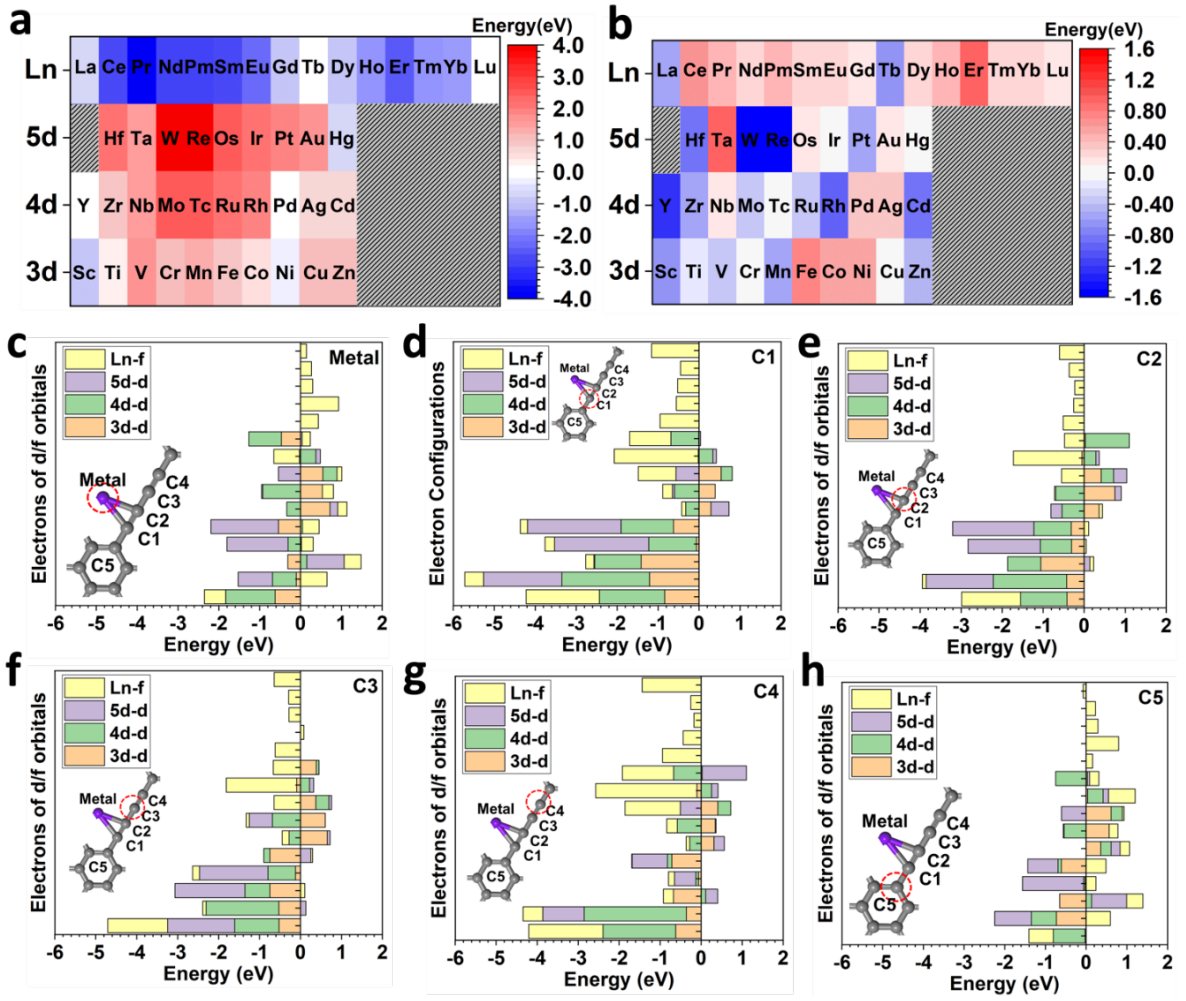

Figure 1. The analysis of CO_2 adsorption on GDY-SACs. The correlation between the (a) formation energy and (b) CO_2 adsorption on the GDY-SACs. The adsorption energies of CO_2 on (c) Metal, (d) C1, (e) C2. (f) C3, (g) C4 and (h) C5 sites of GDY-SACs.

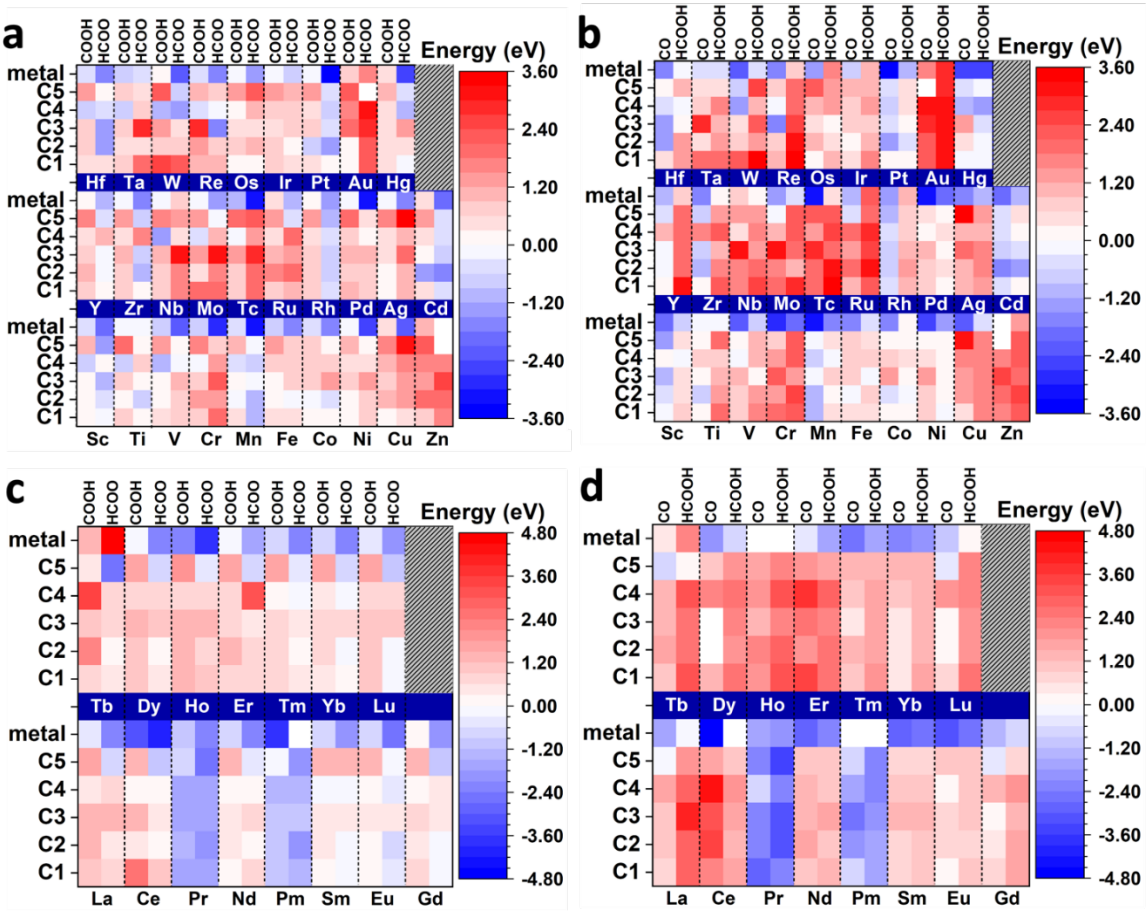

Figure 2. The reaction energy change of CO_2 transitions to HCOOH and CO. (a) Formation of HCOO* and COOH* from CO_2 and (b) Formation of CO and HCOOH on GDY-TMs SAC. (c) Formation of HCOO* and COOH* from CO_2 and (d) Formation of CO and HCOOH on GDY-Ln SACs.

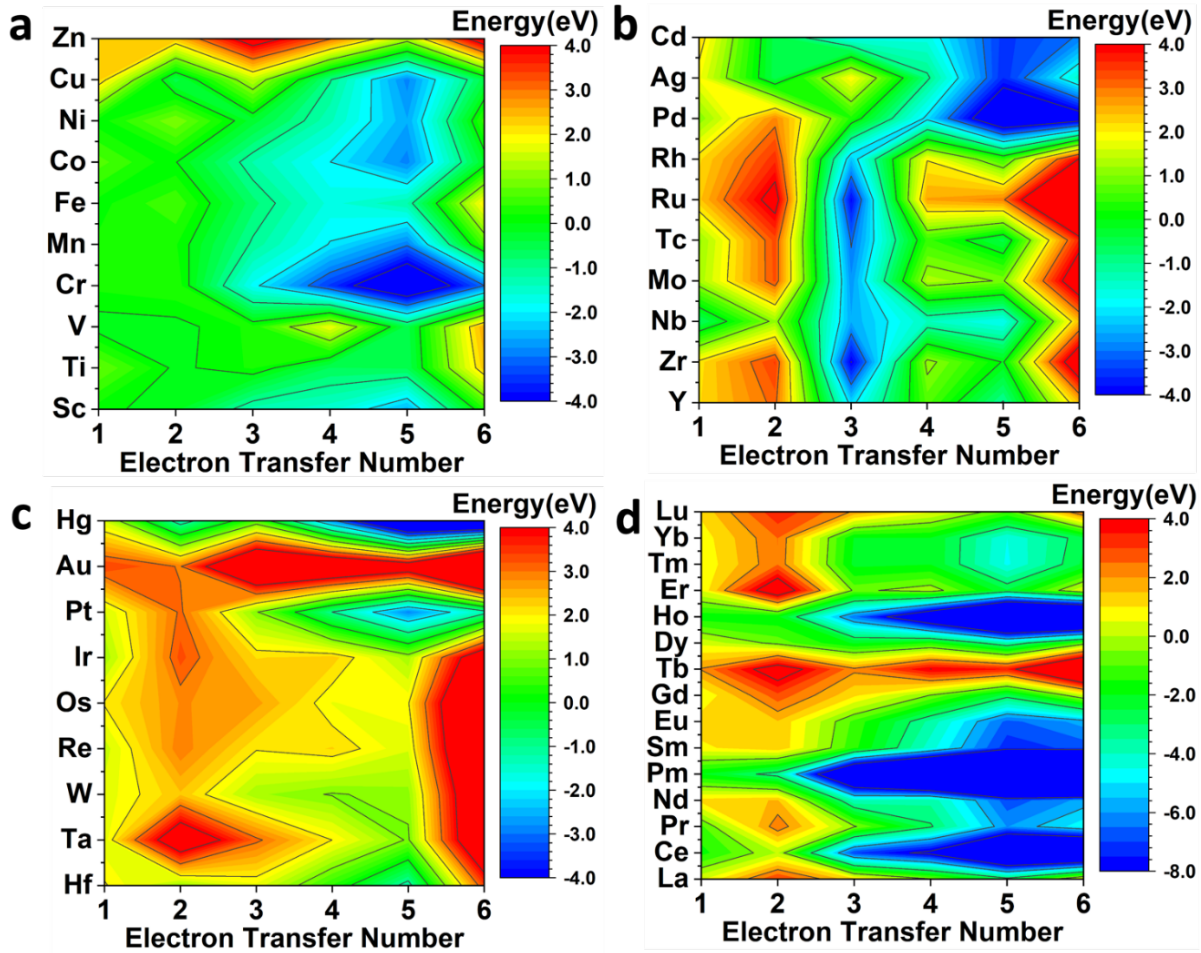

Figure 3. The reaction pathways of CO transition to CH_4 with the lowest energy change. (a) GDY-3d TMs SAC. (b) GDY-4d TMs SACs. (c) GDY-5d TMs SACs. (d) GDY-Ln SACs.

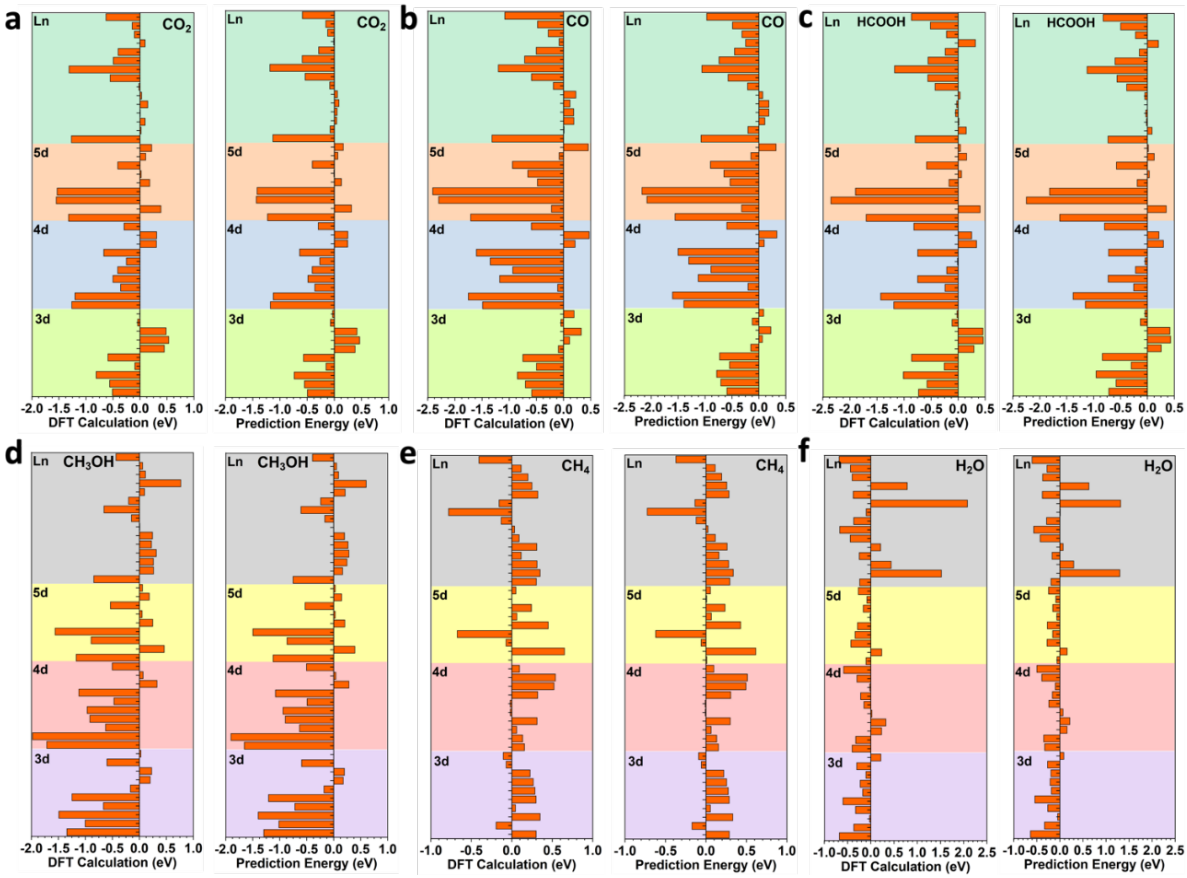

Figure 4. Machine learning predictions of different intermediates with neighboring effects. (a) CO_2, (b) CO, (c) HCOOH, (d) CH_3OH, (e) CH_4 and (f) H_2O. Left panel: DFT calculation results. Right Panel: machine learning results.